Nonlinear Sequence-Dependent Structure of Nigral Dopamine Neuron Interspike Interval Firing Patterns

Ralph E. Hoffman,* Wei-Xing Shi,* and Benjamin S. Bunney*‡
*Department of Psychiatry, Yale University School of Medicine, and ‡Department of Pharmacology, Yale University School of Medicine, New Haven, Connecticut USA

ABSTRACT Firing patterns of 15 dopamine neurons in the rat substantia nigra were studied. These cells alternated between two firing modes, single-spike and bursting, which interwove to produce irregular, aperiodic interspike interval (ISI) patterns. When examined by linear autocorrelation analysis, these patterns appeared to reflect a primarily stochastic or random process. However, dynamical analysis revealed that the sequential behavior of a majority of these cells expressed "higher-dimensional" nonlinear deterministic structure. Dimensionality refers to the number of degrees of freedom or complexity of a time series. Bursting was statistically associated with some aspects of nonlinear ISI sequence dependence. Controlling for the effects of nonstationarity substantially increased overall predictability of ISI sequences. We hypothesize that the nonlinear deterministic structure of ISI firing patterns reflects the neuron's response to coordinated synaptic inputs emerging from neural circuit interactions.

INTRODUCTION

Dopamine (DA) neurons in the substantia nigra are thought to help regulate sensorimotor integration by mammalian striatal systems (Alexander and Crutcher, 1990; Marshall and Gotthelf, 1979; Schneider, 1991; Vives and Mogenson, 1986). Nigral DA neurons have two modes of firing: single-spike and bursting (Bunney et al., 1973; Grace and Bunney, 1984a, b). Single-spike mode firing yields interspike intervals (ISIs) that vary widely and appear random, whereas bursting consists of one or more relatively reduced ISIs followed by an extended ISI. Bursting induces large increases in postsynaptic efficacy not accounted for by changes in firing rate (Gonon, 1988; Bean and Roth, 1991). Measures of DA neuron behavior generally assume stochastic (random) firing with some central tendency, e.g., mean firing rate or percent spikes in bursts, appraised by statistical averaging.

However, burst and single-spike firing modes interweave to produce irregular ISI patterns that statistical averaging ignores. ISI patterns of nigral DA neurons reflect interactions with nonnigral neural circuitry. This is demonstrated by recordings of DA cells in in vitro slice preparations where nonnigral inputs have been eliminated. Under these conditions variability of ISIs is dramatically reduced (Sanghera et al., 1984; Shepard and Bunney, 1988; Silva and Bunney, 1988).

Many neuronal systems express deterministic properties by virtue of rhythmic behaviors detectable by linear analyses such as the power spectrum or the autocorrelation function (Chang et al., 1994). Dynamical analysis has now provided tools that can also detect *nonlinear* deterministic properties of time series. Such determinism produces irregular, aperiodic behavior that traditional linear analyses would interpret as stochastic or random (Chang et al., 1994; Sugihara and May, 1990; Tsonis and Elsner, 1988; Tidd et al., 1993). Nonlinear methods have recently been used to study the behavior of neurons and neuronal ensembles (Longtin, 1993; Chang et al., 1994; Schiff et al., 1994; Rapp et al., 1994). Computer models of even very simple neural networks suggest that firing patterns of neurons will exhibit sequence-dependent nonlinearities owing to circuit interactions (Chapeau-Blondeau and Chauvet, 1992; Lewis and Glass, 1992). Nonlinear deterministic behavior may have physiological or computational significance distinct from oscillatory processes.

Chang et al. (1994) found oscillatory linear structure in 4/4 recordings of cat spinal cord motoneuron ensembles recorded in the decerebrate state and nonlinear structure in 2/4 of these recordings. In contrast, five motoneuron ensembles demonstrated neither linear nor nonlinear structure when studied in the spinalized state where circuitry providing input to these cells is significantly curtailed. Schiff et al. (1994) detected nonlinear structure in 1/6 populations of hippocampal cells in slice preparations that were induced to burst spontaneously by potassium perfusion. Rapp et al. (1994) demonstrated greater levels of ISI nonlinear structure in spontaneously firing rat cortical neurons relative to activated states secondary to penicillin epileptogenesis. In the former group, 4/7 cells demonstrated statistically significant evidence of nonlinear structure.

The prevalence of nonlinear determinism expressed by a larger sample of neurons of a particular type remains unexplored. DA cells are of special interest because they spontaneously produce richly textured ISI patterns, and their physiological properties have been extensively studied (for a review see Bunney et al., 1991). Therefore our first goal was to assess to the prevalence and nature of sequence-

Received for publication 17 November 1994 and in final form 6 February 1995.

Address reprint request to Ralph Hoffman, M.D., Yale Psychiatric Institute, P.O. Box 208038, New Haven, CT. 06520-8038 Tel.: 203-785-7260; Fax: 203-785-7855; E-mail: hoffman@biomed.med.yale.edu.

© 1995 by the Biophysical Society

0006-3495/95/07/128/10 $2.00

dependent nonlinearities for an expanded sample of these neurons.

Our second goal was to estimate, at least roughly, the "dimensionality" of DA neuron firing patterns. Dimensionality is a measure of complexity that correlates with the number of degrees of freedom of a time series—in other words, the number of essential variables needed to model dynamical processes producing the behavioral fluctuations measured over time (Denton and Diamond, 1991; Farmer et al., 1983; Rapp et al., 1985).

Our third goal was to assess the relationship between bursting and nonlinear structure of ISI sequences. Many cell types exhibit burst firing where activation momentarily predisposes the cell to further activation (Bunney et al., 1991; Freeman and Bunney, 1987; Legendy and Salcman, 1985; Sparks and Mays, 1980; White et al., 1989; Wong and Prince, 1981; Wong and Stewart, 1992). In DA neurons, bursting is likely to reflect, at least in part, intracellular calcium influx, which promotes additional spike activity (Grace and Bunney, 1984b). It is possible therefore that nonlinear structure of DA neuron ISIs arises primarily from burst-associated physiological properties of the neuron itself rather than from the temporal organization of its synaptic inputs.

Our fourth goal was to assess whether nonstationarity altered our assessments of deterministic structure. It is possible that ISI firing patterns lack a clearly fixed mean; if so, assessments of deterministic structure should control for this factor.

MATERIALS AND METHODS

Experimental preparation

We studied Sprague–Dawley rats weighing 160–300 g, using low cerveau isolé preparations (Bunney and Aghajanian, 1976; Sesack and Bunney, 1989). The brain stem was transected after the animal was initially anesthetized with halothane, and then locally anesthetized by infiltration of a long-acting local anesthetic, 2% mepivcaine hydrochloride, at all pressure points and incision sites. A small burr hole was drilled 2 mm caudal to the lambdoidal suture and 1 mm medial to the bony ridge at the lateral edge of the skull. To transect the brain stem, a 30-gauge, half-in. needle was inserted at a 30-deg angle relative to the coronal plane and rotated, parallel to the lambdoidal suture, until the needle was at a 90-deg angle. Halothane anesthesia was discontinued for at least 30 min before physiological recordings were generated. Throughout the recording period, body temperature was maintained at 35–38°C.

Single unit activity of DA neurons in the substantia nigra was monitored as described previously (Bunney et al., 1973). Glass microelectrodes were made by using a Narishiga electrode puller and filled with 1-M NaCl solution containing 2% Pontamine Sky Blue dye. The tip of the electrode was broken back under microscopic examination to a diameter of 1–3 μm and resistance established between 5 and 15 MΩ. A small burr hole was drilled above the substantia nigra (2.5 mm anterior to the lambdoidal suture and 2.0 mm lateral to the midline), and the electrode was lowered 6.5–8.5 mm below the cortical surface.

Spike identification and calculation of interspike intervals utilized modified LabView Data Acquisition software (National Instruments, Austin, TX) and a PC$^+$ interface (National Instruments) linked to an IBM-486 compatible computer.

DA neurons were identified based on well-established criteria (Bunney et al., 1973, Grace and Bunney, 1980, 1983) including i) anatomic location in the substantia nigra zona compacta region, ii) a distinctive extracellular action potential waveform of long duration (1.8 to 4 ms) with initially positive action potentials followed by a prominent negative component, iii) characteristic firing patterns consisting of either irregularly distributed single spikes or bursts with spikes of decreasing amplitude and increasing duration, and iv) firing rate typically of 2 to 8 Hz.

Spike identification occurred if the action potential exceeded a positive height threshold set to capture all spikes generated by the cell being studied but clearly exceeding the random fluctuations of baseline signal potentials. Data collection was not initiated until the absence of drift in action potential height was clearly established. Recordings were then continuously screened during data collection to ensure that action potential height and baseline noise level did not change.

Batch processing by our software required a uniform data set size, which was set at 2100 and 2400 ISI events. The refractory period of DA cells was assumed to be approximately 10 ms (Grace and Bunney, 1980; Yeomanns et al., 1988). Consequently any data sets with ISIs < 10 ms were not further analyzed. To be included in the study, cells were required to have evidence of greater than 10 occurrences of bursting. Bursts were defined in the standard fashion, namely, an initial ISI < 80 ms optionally followed by later ISIs of <160 ms (Grace and Bunney, 1984b). Beyond meeting these criteria, cells were selected randomly for analysis. Two cells were rejected because of insufficient bursting, and seven cells were rejected because of ISIs of <10 ms. This left a total of 15 nigral DA cells which met our inclusion criteria and formed the ISI database for our study.

Mathematical background

In general, the simplest type of sequence-dependent time series structure consists of combinations of periodic oscillations that can be represented as follows:

$$x_t = \sum_{i=1}^{n} \alpha_i * x_{t-i} + \epsilon, \quad (1)$$

where x_t is the most recent event, x_{t-i} is the event for the ith step in the past, α_i is the corresponding linear prediction coefficient, and ϵ is Gaussian noise (Theiler et al., 1992). A more complex form of sequence-dependent structure is the following:

$$y_t = h(x_t), \quad (2)$$

where x_t is an input function represented in Eq. 1 and the output, y_t, is a distortion of x_t derived from a nonlinear function h (Theiler et al., 1992). Time series of this sort are said to have static nonlinear structure. In contrast, sequence-dependent nonlinear structure has the following general form:

$$x_t = f(x_{t-1}, x_{t-2}, \ldots, x_n) + \epsilon, \quad (3)$$

where f is a nonlinear function with arguments corresponding to one or more events occurring at different points in the system's history (Nychka et al., 1992). Each of these three types of time series has sequence-dependent structure. The challenge is differentiating the first two varieties, which emerge from stochastic noise and linear oscillations, from sequence-dependent nonlinearity reflected by Eq. 3.

Assessing sequence-dependent structure

Linear structure was assessed by using the autocorrelation function, which calculates the linear correlation of a time series with itself across different event lags (the "delay" in terms of number of events or ISIs used to create an alternative data set that is correlated with the original data set; Box and Jenkins, 1976; see also Appendix A1).

We used two different approaches for detecting nonlinear sequence-dependent structure of ISI firing patterns.

The first approach is referred to as *nonlinear prediction* (Longtin, 1993; Chang et al., 1994; Schiff et al., 1994). Given an index set of observations x_t, x_{t+1}, ... x_{t+n-1} belonging to $\{x_t\}$, the task is to predict the next observation, x_{t+n}. Alternative sequences of observations in the data set $\{x_t\}$ similar to the index sequence are sought, and an average of their movements to next observations is computed. This average is compared with actual observed event, x_{t+n} (see Appendix A3 for details).

Our second approach maps a sequence of observations $\{x_t\}$ into a set of n-dimensional state vectors $\{\mathbf{x}_t\}$ according the following process: x_t is the first coordinate, x_{t+1} is the second coordinate, etc., with x_{t+n-1} being the last coordinate (Grassberger and Procaccia, 1983; Tsonis and Elsner, 1988). Thus a sequence of observations is translated into a "cloud" of points in the state space. Any pair of these points has a measurable distance separating them. "From this 'cloud' the number of pairs can be found, $N(r, n)$ with distances less than r" (Tsonis and Elsner, 1988). The variable r can therefore be thought of as a spatial cutoff that determines whether different points in the n-dimensional space are counted as neighbors (see Appendix A2 for details). For data sets with significant sequence-dependent structure, the expansion of $N(r, n)$ occurs more "gently," i.e., over a much larger domain of r, than for an observational set with the same distribution sequenced randomly. If, for significantly small r,

$$N(r, n) \propto r^d,$$

then d, the scaling exponent, estimates *correlational complexity* of the observed sequence relative to the embedding dimension n (Tsonis and Elsner, 1988; see also Appendix A2).

Our strategy for detecting nonlinear structure also utilized Gaussian-scaled surrogates of data sets (Rapp et al., 1993; Theiler et al., 1992; Chang et al., 1994; see Appendix A3 for the algorithm). These surrogate data sets approximate linear correlative structure (Eq. 1) and duplicate static monotonic nonlinearity (Eq. 2) while destroying sequence-dependent nonlinear structure (Eq. 3). Our criterion measurements of determinism (nonlinear prediction and correlational complexity) were applied to each original data set and 10 corresponding Gaussian-scaled surrogates. To estimate prominence of such nonlinearity for individual data sets, S scores were calculated (Theiler et al., 1992; Rapp et al., 1993). For nonlinear prediction

$$S = (p_o - \langle p_s \rangle)/\sigma_s, \tag{4a}$$

where p_o is the predictability of the original data set and $\langle p_s \rangle$ and σ_s are the mean and the standard deviation of predictability of the 10 corresponding surrogates. If predictive nonlinearity were present, p_o should be greater than p_s.

For correlational complexity, S scores were calculated as

$$S = (\langle C_s \rangle - c_o)/\sigma_s, \tag{4b}$$

where $\langle c_s \rangle$ is the mean correlational complexity of the 10 surrogates, c_o is the correlational complexity of the original data set, and σ_s is the standard deviation of the surrogates. If correlational nonlinearity were present, c_o should be less than c_s.

S values are expressed as "sigmas" because they are scaled against σ_s. As suggested by Longtin (1993), an S value of three or more sigmas was interpreted as indicating significant sequence-dependent nonlinearity for individual cells.

Surrogate methods for assessing sequence-dependent structure were tested initially by Chang et al. (1994) using the Hénon map, a completely deterministic "low-dimensional" system based on two variables and a single nonlinear component. Neuronal behavior may not reduce to such mathematical simplicity, however. Therefore we wished to assess the ability of our two structural measures, combined with Gaussian-scaled surrogates, to detect sequence-dependent nonlinearity by using known formal systems with higher dimensionality and with noise contamination. For this purpose we used second-order approximations of the Mackey–Glass differential equation (Grassberger and Procaccia, 1983, p. 207)

$$\frac{dx(t)}{dt} = \frac{ax(t-\tau)}{1 + [x(t-\tau)]} - bx(t), \tag{5}$$

where $a = 0.2$, $b = 0.1$, and τ is varied. Time series generated with $\tau = 23$ and $\tau = 100$ are illustrated in Fig. 1, *A* and *B*. They correspond to nonlinear "chaotic" systems with dimensionality roughly equal to 2.4 and 7.5 (Grassberger and Procaccia, 1983). To assess the sensitivity of this method in detecting higher-dimensional nonlinearity, two different 7.5-dimensional Mackey–Glass time series were summed to create a time series with putative dimensionality of 15 (Fig. 1 *C*). A fourth time series was generated by adding Gaussian noise to the 2.4-dimensional Mackey–Glass system such that the amplitude of former was 70% of the latter (Fig. 1 *D*).

After demonstrating that our methods could detect higher-dimensional and noise-contaminated nonlinearity, we applied them to ISI data sets generated by DA cells. Also calculated were the mean and the standard deviation of ISIs within each data set, skewness of ISI distributions, and percent of spikes in bursts.

Finally we wished to assess the effects of nonstationarity that were due to local shifts in mean ISI (see Fig. 3 *A*, for example). This was accomplished by "first-differencing" each data set, i.e., x_1, x_2, ... x_m is transformed into $x_1 - x_2$, $x_2 - x_3$, ..., $x_{m-1} - x_m$. Dynamical analyses of first-differenced data sets were then repeated (Box and Jenkins, 1976; Sugihara and May, 1990).

All tests of statistical significance were two-tailed.

RESULTS

Mackey–Glass systems

The results of our methods applied to 2400-element Mackey–Glass data sets are listed in Table 1. As "true dimensionality" increased, correlational complexity increased and nonlinear prediction decreased. Both measures of sequence-dependent structure combined with Gaussian-scaled surrogates performed well in detecting noise-free Mackey–Glass nonlinearity, even with dimensionality of 15. S values remained seven sigmas or above when both structural measures and both embedding dimensions were used. However, nonlinear prediction was somewhat more robust than correlational complexity in detecting Mackey–Glass nonlinearity embedded in noise; S values generated by the complexity method were less than seven sigmas, whereas S values generated by the prediction method remained greater than seven sigmas.

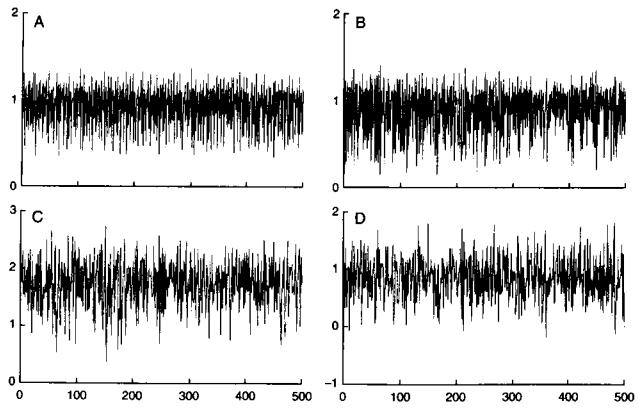

FIGURE 1 Four different Mackey–Glass data sets: *A*, a 2.4-dimensional system; *B*, a 7.5-dimensional system; *C*, the sum of two different 7.5-dimensional systems; *D*, the sum of a 2.4-dimensional system and noise whose amplitude is 70% of the former. The *X* axis corresponds to number of time series events. The irregularity of time series appears to increase as dimension increases or with the addition of noise.

TABLE 1 Dynamical analyses of Mackey–Glass systems based on comparisons with Gaussian-scaled surrogates*

	MG-2.4		MG-7.5		MG-15		MG-2.4+N‡	
Embedding Dimension	r_s‖	S¶	r_s‖	S¶	r_s‖	S¶	r_s‖	S¶
Nonlinear prediction								
4	0.95	68.7	0.80	40.0	0.47	7.17	0.38	12.0
7	0.94	48.8	0.66	24.4	0.51	8.54	0.39	8.37
Correlational complexity	c†	S§	c†	S§	c†	S§	c†	S§
4	1.92	71.9	2.63	38.6	3.4	7.01	3.27	2.35
7	2.09	86.6	3.72	40.8	5.01	8.16	5.21	6.70

*MG number refers to the dimensionality of the formal Mackey–Glass system.
‡2.4-Dimensional Mackey–Glass system plus noise whose amplitude is 70% of the former.
‖Spearman-rank correlation between observed and predicted events.
¶Sigma scores calculated on the basis of 10 surrogates and Eq. 4a.
†Correlational complexity.
§Sigma scores calculated on the basis of 10 surrogates and Eq. 4b.

DA cell data analysis

Fig. 2 illustrates ISI progressions for four representative DA cells. Compared visually with Mackey–Glass formal systems illustrated in Fig. 1, ISI data sets appeared to demonstrate irregularity consistent with higher dimensionality or significant noise contamination. Fig. 3 illustrates the fine structure of this progression for one cell with demarcation of burst periods. Table 2 provides standard descriptive data for the 15 cells.

Autocorrelation analysis of the ISI data sets revealed only traces of linear structure most commonly expressed as small adjacent event (i.e., lag equaling 1) negative autocorrelations. However, no significant oscillatory resonances were detected for any cell. Representative autocorrelation functions are illustrated for three cells in Fig. 4 *A*. Autocorrelations were also calculated for Gaussian-scaled surrogates. The linear structure of the latter was found to approximate successfully the linear structure of original ISI data sets (see Fig. 4 *B*).

Mean ± SD nonlinear prediction scores for ISI data sets (corresponding to values of r_s averaged across the 15 cells) was 0.25 ± 0.09 for an embedding dimension of 4 and 0.24 ± 0.09 for an embedding dimension equal to 7. These measures were considerably lower than those produced by

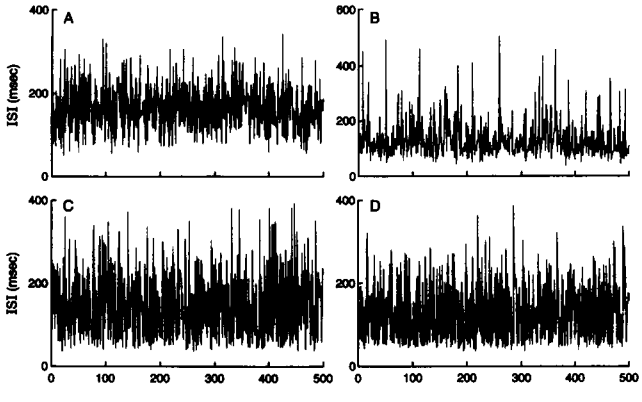

FIGURE 2 Representative subsets of ISI progressions for four different DA cells. The X axis corresponds to ISI events. *A* has relatively few bursts, whereas *B–D* have relatively high burst penetration. *B* is somewhat unusual insofar as ISIs are tightly clustered within the 100–200-ms range but much longer ISIs (>400 ms) occur episodically.

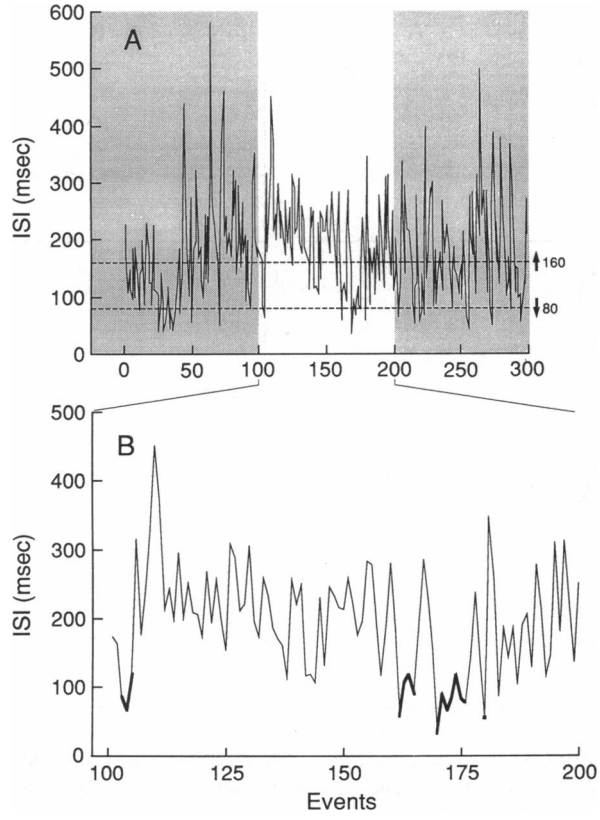

FIGURE 3 Demarcation of bursts. *A*, Blow-up of 300 consecutive ISIs. Dashed lines reflect thresholds for entering and exiting bursts. Some drift in the mean ISI seems apparent at this level of detail. *B*, More-detailed view of the middle 100 ISIs. The square denotes a two-spike burst. Heavy lines denote more extended burst periods. The reduced ISIs of a burst are immediately followed by an extended ISI that exceeds the local mean. This pattern could be a source of sequential structure.

TABLE 2 Characteristics of DA cells (N = 15)

Characteristic	Mean ± SD	Range
Mean ISI*	162 ± 30	130–246
ISI variability‡	83.7 ± 25.6	52.5–142.2
Skewness	1.08 ± 0.86	0.11–2.93
% Spikes in bursts	26.8 ± 16.4	2.3–47.1

*In milliseconds.
‡Calculated as standard deviations.

any of the Mackey–Glass systems that we studied (see Table 1). Mean ± SD correlational complexity was 3.21 ± 0.21 for an embedding dimension of 4 and 4.61 ± 0.70 for an embedding dimension of 7, which fell between correlational complexities for the Mackey–Glass 7.5- and 15-dimensional systems (see again Table 1).

The null hypothesis that ISI progressions reflect noise conditioned by linear autocorrelation and static monotonic nonlinearity was tested. Pairwise t-tests reflecting the difference between nonlinear prediction scores of raw data for all 15 cells and mean prediction scores of their corresponding Gaussian-scaled surrogates were strongly significant for an embedding dimension equal to 4 (t = 5.79, df = 14, $p <$ 0.0005) and an embedding dimension equal to 7 (t = 4.94, df = 14, $p <$ 0.0005). Pairwise t-tests reflecting the difference between correlational complexity scores of raw data and mean scores of surrogates were also strongly significant for an embedding dimension equal to 4 (t = 5.94, df = 14, $p <$ 0.0005) and moderately significant for an embedding dimension equal to 7 (t = 2.58, df = 14, $p <$ 0.05). Therefore the null hypothesis can be rejected with a high level of confidence.

Fig. 5 illustrates corresponding S scores for individual cells. Using a cutoff S value of three sigmas, nonlinear prediction identified nonlinear sequential ISI structure in a total of 10 out of 15 cells for both embedding dimensions. There was some disagreement in classifying individual cells, however. An embedding dimension of 7 identified cell 1 as having significant nonlinear structure, whereas cell 2 had a sigma score below the cutoff. An embedding dimension of 4 reversed the classification of these two cells. Classifications of the remaining 13 cells were identical based on the two embedding dimensions. Correlational complexity detected nonlinear structure in a total of 9 out of 15 cells for both embedding dimensions. There was disagreement in classifying 3 of 15 individual cells (cells 2, 10, and 15; see again Fig. 5) when complexity-based sigma scores were compared for the two embedding dimensions. S values generated by nonlinear prediction versus correlational complexity for particular embedding dimensions did not correlate at a statistically significant level (for an embedding dimension equal to 4; Spearman rank r_s = 0.23; for an embedding dimension equal to 7, r_s = 0.45).

The effects of bursting on the expression of nonlinear structure were assessed by computing correlations between S scores and other characteristics of ISI data sets (Table 3). Three of four measures of nonlinearity yielded positive

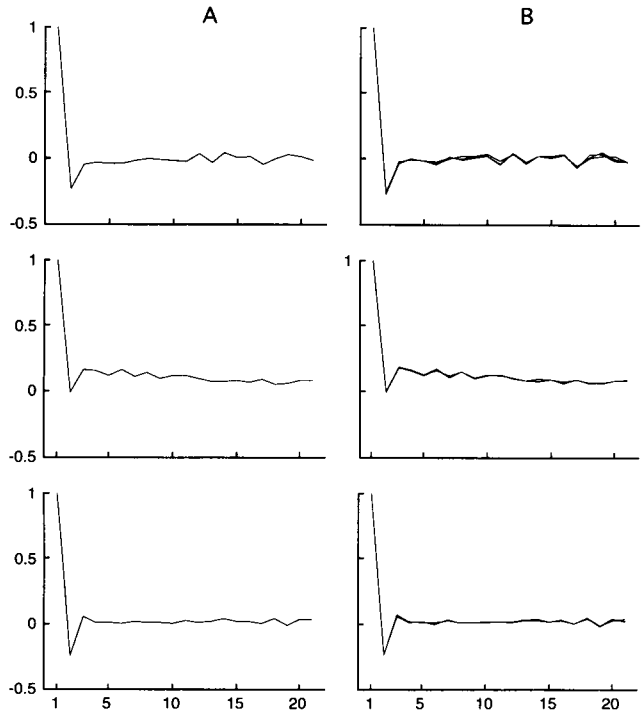

FIGURE 4 A, Autocorrelation functions for three representative ISI data sets. The first and third cells began with a small negative autocorrelation for adjacent events but converged in a "noiselike" fashion to near-zero levels at larger event lags. The second cell demonstrated a near-zero autocorrelation for event lag of one with small positive correlations for later phase lags. None of the three cells generated evidence of sustained oscillatory organization. B, Corresponding autocorrelation functions for three Gaussian-scaled surrogates for each of the three data sets; surrogates overlap extensively and are often not distinguishable. The linear structure in A is closely approximated by the surrogates.

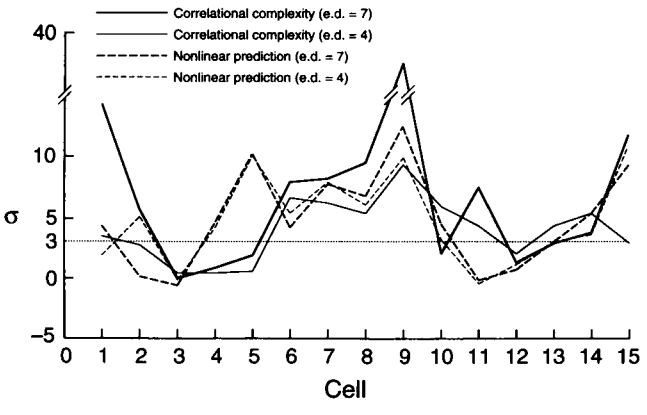

FIGURE 5 S scores for the 15 neurons calculated for nonlinear prediction and correlational complexity measures of determinism and both embedding dimensions. For nonlinear prediction, the mean ± SD S score equaled 4.80 ± 4.71 for an embedding dimension of 4 and 5.14 ± 4.78 for an embedding dimension of 7. For correlational complexity, mean ± SD S scores equaled 3.92 ± 2.56 for an embedding dimension of 4 and 8.07 ± 9.10 for an embedding dimension of 7. The dotted line represents the S score cutoff of three sigmas. Other dynamical measure methods sometimes identified different cells as having nonlinear structure (see, for instance, cells 5 and 11).

TABLE 3 Spearman-rank correlations between nonlinearity measures (*S* scores) and ISI characteristics*

	Nonlinear Prediction		Complexity	
Characteristic	e.d. = 4	e.d. = 7	e.d. = 4	e.d. = 7
Mean ISI	−0.26	−0.38	−0.59	−0.23
ISI SD	0.55	0.48	−0.11	0.04
Skewness	−0.17	0.22	−0.17	−0.24
% Spikes in bursts	0.61	0.69[§]	0.53	0.16

*e.d., Embedding dimension.
[§]$p < 0.01$.

correlations between *S* scores and percent of spikes in bursts; however, when a *p*-value criterion of 0.01 that was due to multiple statistical comparisons was used, only one of these correlations reached statistical significance. Moreover, the surrogates used in this study also demonstrated "bursting" as defined formally in the Methods section. Mean burst length (counted as number of spikes) was computed for each DA cell and its surrogates. Burst length was found to be slightly reduced in surrogates relative to actual cells, but not significantly so (3.17 ± 0.72 spikes for surrogates, 3.32 ± 0.87 spikes for cells, $t = 1.81$, $df = 14$, $p < 0.10$). These findings suggest that sustained excitability resulting from bursting is unlikely to be the sole source of sequence-dependent nonlinear structure. Correlations between *S* scores and other characteristics of ISI data sets were computed (Table 3). Mean, standard deviation, and skewness of ISIs did not produce statistically significant correlations with sigma scores.

To assess the effects of nonstationarity, all analyses were repeated for first-differenced data sets. There was a noteworthy shift in adjacent event autocorrelation scores. Whereas original data sets sometimes demonstrated small adjacent event autocorrelations (mean ± SD = −0.08 ± 0.19), adjacent event autocorrelations of differenced data were consistently and robustly negative (mean ± SD = −0.53 ± 0.09; see Fig. 6 *A* for examples). Autocorrelations at larger event lags quickly collapsed to near zero, suggesting a near-stochastic sequential process.

Corresponding increases in predictability of first-differenced data sets were also observed (Fig. 7, top). The mean ± SD nonlinear prediction score for an embedding dimension of 4 increased to 0.64 ± 0.08 (from 0.25 ± 0.09 for untransformed data sets). The mean ± SD nonlinear prediction score for an embedding dimension of 7 increased to 0.59 ± 0.07 (from 0.24 ± 0.09 for untransformed data sets). However, mean correlational complexity measures changed little for first-differenced data sets relative to untransformed data sets (3.19 versus 3.21 for an embedding dimension of 4 and 4.47 versus 4.61 for an embedding dimension of 7; see Fig. 7, bottom). Mean correlational complexity and nonlinear prediction measures of differenced ISI data sets all fell between those of the 7.5-dimensional and the 15-dimensional Mackey–Glass system (see Table 1).

Autocorrelation analysis again demonstrated that Gaussian-scaled surrogates successfully approximated linear

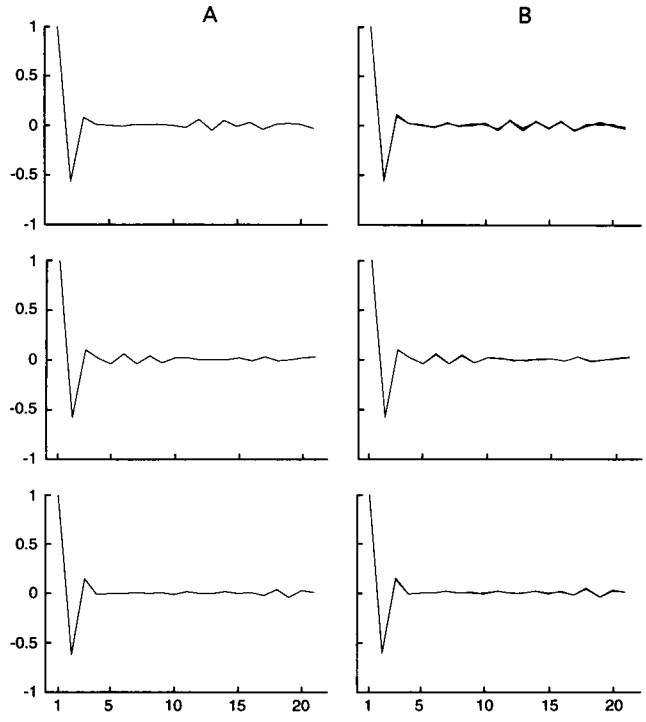

FIGURE 6 *A*, Autocorrelations for first-differenced data sets for the same three cells illustrated in Fig. 4. Autocorrelation at the first event lag is now consistently and robustly negative. For cell 2, persistent positive autocorrelations have disappeared, suggesting that they were due to drift in mean ISI. Sustained oscillatory trends are still not evident. *B*, Autocorrelations for three (largely overlapping) Gaussian-scaled surrogates for each of these cells. Once again, linear structure represented in *A* is closely approximated by surrogates.

structure of first-differenced data sets (Fig. 6, *B*). There was little change in the extent to which nonlinearity was delineated by surrogate analysis of first-differenced data. Mean sigma scores were roughly unchanged; for each of the four dynamical variables (nonlinear prediction and correlational complexity calculated for the two embedding dimensions) 9/15 cells demonstrated statistical evidence of nonlinear structure with sigma scores exceeding three. For nonlinear prediction, mean ± SD *S* score equaled 5.39 ± 6.99 for an embedding dimension of 4 and 3.89 ± 4.33 for an embedding dimension of 7. For correlational complexity, mean ± SD *S* scores equaled 6.08 ± 5.12 for an embedding dimension of 4 and 6.86 ± 5.11 for an embedding dimension of 7. No correlation between sigma scores for first-differenced data and percent bursting achieved statistical significance at a 0.01 criterion level (values of r_s ranged from 0.18 to 0.59). Spearman-rank correlations between sigma scores for first-differenced data and other characteristics of ISI data sets (mean, standard deviation, and skewness of ISIs) were also not statistically significant.

DISCUSSION

Testing our methods with formal Mackey–Glass systems demonstrated that both nonlinear prediction and correla-

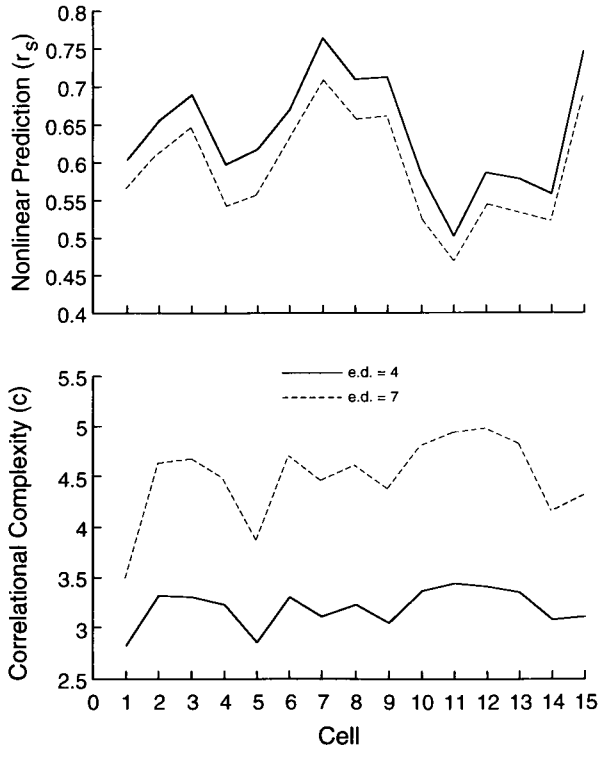

FIGURE 7 Nonlinear prediction and correlational complexity scores for the 15 ISI data after first-differencing. Different embedding dimension produced very consistent shifts in these two dynamical measures.

tional complexity are sensitive to higher-dimensional nonlinear structure. A somewhat surprising finding was that the former was more robust in detecting nonlinear structure embedded in noise. Perhaps this reflects the fact that nonlinear prediction includes an averaging procedure that buffers noise effects.

Our central empirical finding was that the 15 DA cells, considered as a group, yielded robust statistical evidence of nonlinear sequential structure. Nonlinear prediction and complexity measures of nigral DA cell ISI time series were different from identical measures applied to surrogate data sets with a high level of statistical certainty for both embedding dimensions. S values for individual neurons were greater than three sigmas in a majority of cells evaluated by both deterministic measures and two different embedding dimensions.

Significant nonstationarities were found in our data. The fact that nonlinear prediction scores more than doubled after differencing ISI data sets indicates that these data often lacked a fixed mean. The major effect of this transformation was to highlight linear rather than nonlinear structure, however. This is reflected in the much more robust adjacent event autocorrelations induced by differencing data and the fact that this transformation did not produce any increase in sigma scores.

First-differencing ISI data provided correlational complexity and nonlinear prediction scores whose means consistently fell between means for the same variables calculated for 7.5- and 15-dimensional Mackey–Glass systems using the same embedding dimensions and data set sizes. These findings suggest that the dimensionality of sequential structure expressed by DA neurons recorded using low cerveau isolé preparations may have had a similar range. Significant levels of stochastic noise added to deterministic processes, however, cannot be ruled out as a factor contributing to erratic ISI patterns and the appearance of higher dimensionality (see again Table 1).

Our interest in linear structure derives from the report by Chang et al. (1994). Only cells in their decerebrate preparations demonstrated evidence of nonlinear structure; these cells also demonstrated prominent oscillatory linear structure, suggesting that nonlinearity delineated by their methods reflected primarily "quasi-periodic" processes. In contrast, the majority of DA cells in our sample demonstrated nonlinear structure even though autocorrelation data did not demonstrate significant periodic organization.

We found that the percentage of spikes in bursts partially correlated with some measures of nonlinear sequential ISI structure. This is consistent with the view that bursting reflects sequence-dependencies, i.e., sustained reductions in ISIs followed by a prolonged ISI (see again Fig. 3). However, these correlative findings were lost when our data sets were first-differenced, even though evidence of nonlinear structure remained. Moreover, an examination of "burst behaviors" of the Gaussian-scaled surrogates demonstrated that burst length was not statistically different compared with that in the original data sets. Thus bursting itself, although it is a conspicuous feature of DA cell behavior in our study, clearly cannot account for *all* sequential nonlinearities detected by our methods.

At least two confounding issues need to be considered when weighing our findings. First, our two measures of determinism produced S values for DA cells that only weakly correlated with each other, suggesting that they reflect different aspects of sequence-dependent structure. This makes intuitive sense. Nonlinear prediction reflects the degree that ISI sequences predict ensuing events. However, there are types of sequential structure that are not at all predictive of future observations. An example is a language that conforms to a particular grammar. One cannot predict which word will follow another in a particular sentence even though word choice is highly constrained (e.g., subject nouns, in general, are followed by verbs). In general, nonlinear prediction varied little when embedding dimension was altered, whereas correlational complexity was very sensitive to embedding dimension. On the other hand, correlational complexity was little changed by differencing data sets but nonlinear prediction was considerably enhanced. It will be important to compare and contrast further the performance of various dynamical measures employed in this and other recent studies (Chang et al., 1994; Schiff et al., 1994; Rapp et al., 1994).

Second, Gaussian-scaled surrogates control for static monotonic nonlinearity (i.e., the h function in Eq. 2) but not for static *nonmonotonic* nonlinearity. Static nonlinear non-

monotonic effects on DA neuron firing are known to occur. For instance, depolarization at times can induce bursting yet at other times block firing by means of depolarization inactivation (Grace and Bunney, 1986; Bunney et al., 1991). The degree to which such effects shape the pattern of DA cell ISIs over time is not known. If these effects are significant, overestimations of sigma scores can result.

As a model to account for our findings, we hypothesize that sequential ISI nonlinearities detected in our study derive from deterministic aperiodic nonnigral synaptic inputs to these cells that are coordinated by larger neural circuit interactions. Some coordinated synaptic inputs may result in pronounced bursting and nonlinear structure, and other coordinated synaptic inputs may induce nonlinear structure even if burst activity is not extensive.

Nigral DA neurons receive excitatory and inhibitory inputs from many interconnected sources (Alexander and Crutcher, 1990), including the corpus striatum (Grace and Bunney, 1985), the dorsal raphe nucleus (Steinbusch and Niewenhuys, 1983), the subthalamic nucleus (Smith and Grace 1992), and other neurons within the substantia nigra itself (Bunney et al., 1991); these inputs are mediated by both chemical neurotransmitters and electrotonic coupling (Bunney et al., 1991; Grace and Bunney, 1985). Coordinated synaptic input yielding sequential nonlinear structure could derive from the collective interactions of these brain areas.

To explore this model in a preliminary fashion we have analyzed ISI data sets from two cells recorded in in vitro slice preparations from which nonnigral synaptic inputs were completely eliminated (R. E. Hoffman, W.-X. Shi, and B. S. Bunney, unpublished data). These data sets retained some variability (ISI standard deviations were 20 and 30 ms, respectively, presumably as the result of intrinsic connections within the substantia nigra or of characteristics of spontaneously firing neurons), although they were much reduced in comparison with ISI data recorded from intact animals (for which ISI standard deviations ranged from 52 to 142 ms). After first-differencing data, significant adjacent event autocorrelations were again detected (-0.39 and -0.40 for the two cells). However, correlational complexities were higher and nonlinear prediction scores were lower than for cells recorded in vivo, and all eight sigma scores (calculated for the two cells, both dynamical measures, and embedding dimensions set at 4 and 7) were less than the cutoff of 3. In short, the cells recorded in slice preparations demonstrated relative reductions in sequential structure (i.e., higher levels of randomness) and an absence of nonlinearity.

Such data do not, of course, provide a definitive test of the model. Dynamical analyses are not required for differentiating in vitro and in vivo recordings of DA cells; this can be accomplished by examining variability of ISI sequences alone. More definitive tests of the model will require selective alterations of one or more major sources of synaptic input to DA neurons recorded in vivo that do not curtail ISI variability or other more standard aspects of cell firing patterns (e.g., percent bursting) that could secondarily affect nonlinear ISI structure. Our prediction is that certain alterations, by virtue of perturbed coordination of synaptic inputs, will eliminate or reduce nonlinear structure of DA cell firing patterns while retaining many standard ISI characteristics. Undertaking such studies will require systematic alterations of different components of neural circuits providing inputs to DA cells.

Our findings indicate that future dynamical studies of ISI patterns will need to consider the confounding effects of nonstationarity and that methodologies should demonstrate a capacity to detect higher-dimensional and/or noise-contaminated nonlinear structure. Keeping these caveats in mind, we anticipate that nonlinear analysis will demonstrate that the moment-to-moment behavior of many types of neuron is not stochastic or random with some central tendency but instead has a sequence-dependent deterministic structure derived from neural circuit interactions.

APPENDIX

A1: Autocorrelation

The autocorrelation function across different spans or lags of ISI events was calculated as follows (Box and Jenkins, 1976; see also Chang et al., 1994):

$$\Psi(L) = \frac{\sum_{t=1}^{N-L} (x_t - \langle x \rangle)(x_{t+L} - \langle x \rangle)}{\sum_{t=1}^{N-L} (x_t - \langle x \rangle)},$$

where L is the event lag, x_t is the ith ISI, N is the total number of ISIs in the data set, and $\langle x \rangle$ is the mean ISI. This calculation can be repeated for any event lag of interest.

A2: Correlational complexity

Estimations of sequence-dependent structure required embedding our data sets of M elements, $\{x_t\}$, into a state space. This was accomplished by mapping $\{x_t\}$ into a set of *lag vectors* $\{\mathbf{x}_t\}$ whose elements were defined as

$$\mathbf{x}_t = (x_t, x_{t+\tau}, x_{t+2\tau}, \ldots, x_{t+(n-1)\tau}),$$

where n was the embedding dimension of the state space and τ was the embedding lag. A number of different methods for choosing an optimal embedding lag have been proposed (Rapp et al., 1988; Fraser and Swinney 1986; Martinerie et al., 1992). We chose autocorrelation time as the criterion (Rapp et al., 1988; Tsonis and Elsner, 1988). Autocorrelation time is defined as the first event lag where the autocorrelation function is less than $1/e$. For all 15 ISI data sets, autocorrelation at one event interval was less than $1/e$. Therefore, τ was set at one for all embeddings.

Correlational complexity was calculated on the basis of the correlation function $N(r, n)$ (Grassberger and Procaccia, 1983, p. 191):

$$N(r, n) = \frac{1}{v^2} \sum_{i,j=i,i\neq j}^{v} \Theta(r - \|\mathbf{x}_i - \mathbf{x}_j\|),$$

where r is a spacing variable, Θ is the Heaviside function (equaling 1 for positive arguments and 0 for negative arguments), v is the total number of lag vectors generated by $\{x_i\}$, and $\| \ldots \|$ is Euclidean distance in the n-dimensional embedding space, where

$$\|\mathbf{x} - \mathbf{y}\| = ((x_0 - y_0)^2 + (x_1 - y_1)^2 + \ldots + (x_{n-1} - y_{n-1})^2)^{1/2}.$$

For large data sets with "fractal" geometric scaling in the embedding space, log ($N(r, n)$) grows linearly with respect to log r. By plotting log $N(r, n)$ against log r, a measure d can be calculated as the slope. This calculation can be repeated multiple times with increasing embedding dimensions n. If d stabilizes with increasing n, it estimates the dimensionality of the dynamical system generating the data set in question.

As dimensionality increases, the number of data points that one requires to estimate it increases exponentially (Eckmann and Ruelle, 1992). We anticipated that the available size of ISI data sets for DA cells would be insufficient to permit us to estimate directly their relatively high dimension. Data sets larger than 3000–4000 ISIs run the risk of significant shifts in state, which could change sequential structure. Consequently we developed a complexity measure analogous to dimensionality calculated relative to particular embedding dimensions but that required fewer data points. For all data sets in our study, plots of log $N(r, n)$ against log r were smoothly sigmoidal with an approximately linear central region. An algorithm was used to estimate the slope of the portion of correlation function curve which was maximally linear. This slope estimation was designated the correlational complexity.

A3: Nonlinear prediction

Nonlinear prediction was calculated as follows:

1. Let $\mathbf{x}_q$ be an element of the set of lag vectors $\{\mathbf{x}_t\}$ generated from an ISI or from surrogate data set $\{\mathbf{x}_t\}$, as described in Appendix A2.

2. Let $\{\mathbf{y}_q\}$ be a subset of $\{\mathbf{x}_t\}$ ($t \neq q$) consisting of the k lag vectors nearest $\mathbf{x}_q$ in terms of Euclidean distance.

3. A prediction of the future event, x_{q+n}, was calculated as the simple average of projections over the k lag vectors:

$$\text{pred}(x_{q+n}) = \frac{1}{k} \sum_{j=1}^{k} y_{j+n},$$

where $\mathbf{y}_j \in \{\mathbf{y}_q\}$ and y_{j+n} is the next ISI occurring "beyond" the lag vector.

Predictions of ISI or surrogate events immediately following each lag vector $\mathbf{x}_q$ were calculated, q ranging from 1 to M–n. To assess the overall predictive success of the algorithm applied across the ISI data set or surrogate, a Spearman-rank correlation coefficient (r_s) was then calculated between the M–n pairs of predictions and corresponding observed events; this nonparametric method of assessing nonlinear prediction accuracy accommodates nonnormal distributions of ISI data sets (many of which were quite skewed; see again Table 2) and was previously used by Sugihara and May (1990). All predictions were generated by using an embedding dimension n set at 4 and 7; k, the number lag vectors used to generated predictions, was set at 2% of the total number of lag vectors in the data set. This same k setting was employed by Chang et al. (1994) and Schiff et al. (1994). Finally, a mean nonlinear prediction score for each embedding dimension was calculating by averaging the 15 values of r_s corresponding to the 15 ISI data sets.

A4: Gaussian-scaled surrogates

Gaussian-scaled surrogates were generated on the basis of a three-step procedure:

1. Assume that $\{x_i\}$ is a time series. A Gaussian-distributed data set with exactly the same number of elements with zero mean and a standard deviation of 1 was created by using a random-number generator. This random data set was then reordered to create $\{y_i\}$ so that its within-set ranks exactly matched the within-set ranks of $\{x_i\}$; in other words, for any q, $y_q \in \{y_i\}$ would have the same rank within its set as the corresponding $x_q \in \{x_i\}$ within its set.

2. $\{y_i\}$ was then Fourier transformed into the frequency domain, and a random phase was added to each term of the Fourier transform. These "phase-randomized" Fourier transforms were then retransformed into the time domain as $\{y'_i\}$. Phase randomization destroys all nonlinear structure (see Eqs. 2 and 3) while approximating linear correlative structure (see Eq. 1).

3. A surrogate data set, $\{x_i'\}$ is created as a reshuffling of the original data set $\{x_i\}$ such that the rank order of all elements belonging to $\{x_i'\}$ matches that of corresponding elements in $\{y'_i\}$. Any static, monotonic nonlinearity (see Eq. 2) intrinsic to $\{x_i\}$ is thus recreated by $\{x_i'\}$. Sequential data sets produced by this shuffling procedure are referred to as *Gaussian-scaled surrogates.*

This research was supported by NIMH grant MH 28849 and the Chrysalis Fund. We wish to acknowledge the assistance of Kenneth Tsai in software development.

REFERENCES

Alexander, G. E., and M. D. Crutcher. 1990. Functional architecture of basal ganglia circuits: neural substrates of parallel processing. *Trends Neurosci.* 30:266–271.

Bean, A. J., and R. H. Roth. 1991. Extracellular dopamine and neurotensin in rat prefrontal cortex in vivo: Effects of median forebrain bundle stimulation frequency, pattern and dopamine autoreceptors. *J. Neurosci.* 11:2694–2702.

Box, G. E. P., and G. M. Jenkins. 1976. Time Series Analysis, Forecasting and Control. Holden-Day, Oakland, CA.

Bunney, B. S., and G. K. Aghajanian. 1976. Dopamine and norepinephrine innervated cells in the rat prefrontal cortex: pharmacological differentiation using microiontophoretic techniques. *Life Sci.* 19:1783–1792.

Bunney, B. S., L. A. Chiodo, and A. A. Grace. 1991. Midbrain dopamine system electrophysiological functioning: a review and new hypothesis. *Synapse.* 9:79–94.

Bunney, B. S., J. R. Walters, R. H. Roth, and G. K. Aghajanian. 1973. Dopaminergic neurons: Effect of antipsychotic drugs and amphetamine on single cell activity. *J. Pharm. Exp. Ther.* 185:560–571.

Chang, T., S. J. Schiff, T. Sauer, J.-P. Gossard, and R. E. Burke. 1994. Stochastic versus deterministic variability in simple neuronal circuits: I. Monosynaptic spinal cord reflexes. *Biophys. J.* 67:671–683.

Chapeau-Blondeau, F., and G. Chauvet. 1992. Stable, oscillatory, and chaotic regimes in the dynamics of small neural networks with delay. *Neural Networks.* 5:735–743.

Denton, T. A., and G. A. Diamond. 1991. Can analytic techniques of nonlinear dynamics distinguish periodic, random and chaotic signals? *Comput. Biol. Med.* 21:243–264.

Eckmann, J.-P., and D. Ruelle. 1992. Fundamental limitations for estimating dimensions and Lyapunov exponents in dynamical systems. *Physica D.* 56:186–187.

Farmer, J. D., E. Ott, and J. A. Yorke. 1983. The dimension of chaotic attractors. *Physica D.* 7:153–180.

Fraser, A. M., and H. L. Swinney. 1986. Independent coordinates for strange attractors from mutual information. *Phys. Rev. A.* 33: 1134–1140.

Freeman, A. S., and B. S. Bunney. 1987. Activity of A9 and A10 dopaminergic neurons in unrestrained rats: further characterization and effects of apomorphine and cholecystokinin. *Brain Res.* 405:46–55.

Gonon, F. G. 1988. Nonlinear relationship between impulse flow and dopamine released by rat midbrain dopaminergic neurons as studied by in vivo electrochemistry. *Neuroscience.* 24:19–28.

Grace, A. A., and B. S. Bunney. 1980. Nigral dopamine neurons: intracellular recording and identification with L-dopa injection and histofluorescence. *Science.* 210:654–656.

Grace, A. A., and B. S. Bunney. 1983. Intracellular and extracellular electrophysiology of nigral dopaminergic neurons—2. Action potential generating mechanisms and morphological correlates. *Neuroscience.* 10:317–331.

Grace, A. A., and B. S. Bunney. 1984a. The control of firing pattern in nigral dopamine neurons: single spike firing. *J. Neurosci.* 4:2866–2876.

Grace, A. A., and B. S. Bunney. 1984b. The control of firing pattern in nigral dopamine neurons: burst firing. *J. Neurosci.* 4:2877–2890.

Grace, A. A., and B. S. Bunney. 1985. Opposing effects of striatonigral feedback pathways on midbrain dopamine cell activity. *Brain Res.* 333:271–284.

Grace, A. A., and B. S. Bunney. 1986. Induction of depolarization block in midbrain dopamine neurons by repeated administration of haloperidol: Analysis using in vivo intracellular recording. *J. Pharm. Exp. Ther.* 238:1092–1100.

Grassberger, P., and I. Procaccia. 1983. Measuring the strangeness of strange attractors. *Physica D.* 9:189–208.

Legendy, C. R., and M. Salcman. 1985. Bursts and recurrences of bursts in the spike trains of spontaneously active striate cortex neurons. *J. Neurophysiol.* 53:926–939.

Lewis, J. E., and L. Glass. 1992. Nonlinear dynamics and symbolic dynamics of neural networks. *Neural Comput.* 4:621–642.

Longtin, A. 1993. Nonlinear forecasting of spike trains from sensory neurons. *Int. J. Bifur. Chaos.* 3:651–661.

Marshall, J. F., and T. Gotthelf. 1979. Sensory inattention in rats with 6-hydroxydopamine-induced degeneration of ascending dopaminergic neurons: apomorphine-induced reversal of deficits. *Exp. Neurol.* 65: 398–411.

Martinerie, J., A. M. Albano, A. I. Mees, and P. E. Rapp. 1992. Mutual information, strange attractors and optimal estimation of dimension. *Phys. Rev. A.* 45:7058–7064.

Nychka, D., S. Ellner, A. R. Gallant, and D. McCaffrey. Finding chaos in noisy systems. *J. R. Statist. Soc. B.* 54:399–426.

Rapp, P. E., A. M. Albano, and A. I. Mees. 1988. Calculation of correlation dimension from experimental data: progress and problems. *In* Dynamic Patterns in Complex Systems. J. A. S. Kelso, A. J. Mandell, and M. F. Schlesinger, editors. World Scientific, Singapore. 191–205.

Rapp, P. E., A. M. Albano, T. I. Schmah, and L. A. Farwell. 1993. Filtered noise can mimic low-dimensional chaotic attractors. *Phys. Rev. E.* 47: 2289–2297.

Rapp, P. E., I. D. Zimmerman, A. M. Albano, G. C. deGuzman, N. N. Greenbaum, and T. R. Bashore. 1985. Experimental studies of chaotic neural behavior: cellular activity and electroencephalographic signals. *In* Nonlinear Oscillations in Biology and Chemistry. H. G. Othmer, editor. Springer-Verlag, Berlin.

Rapp, P. E., I. D. Zimmerman, E. P. Vining, N. Cohen, A. M. Albano, and M. A. Jiménez-Montaño. 1994. The algorithmic complexity of neural spike trains increases during focal seizures. *J. Neurosci.* 14:4731–4739.

Sanghera, M. K., M. E. Trulson, and D. C. German. 1984. Electrophysiological properties of mouse dopamine neurons: in vivo and in vitro studies. *Neurosci.* 12:793–801.

Schiff, S. J., K. Jerger, T. Chang, T. Sauer, and P. G. Aitken. 1994. Stochastic versus deterministic variability in simple neuronal circuits: II. Hippocampal slice. *Biophys. J.* 67:684–691.

Schneider, J. S. 1991. Response of striatal neurons to peripheral sensory stimulation in symptomatic MPTP-exposed rats *Brain. Res.* 544: 297–302.

Sesack, S. R., and B. S. Bunney. 1989. Pharmacological characterization of the receptor mediating electrophysiological responses to dopamine in the rat medial prefrontal cortex: a microiontophoretic study. *J. Pharm. Exp. Ther.* 248:1323–1333.

Shepard, P. D., and B. S. Bunney. 1988. Effects of apamin on the discharge properties of putative dopamine-containing neurons in vitro. *Brain Res.* 463:380–384.

Silva, N. L., and B. S. Bunney. 1988. Intracellular studies of dopamine neurons in vitro: pacemakers modulated by dopamine. *Eur. J. Pharmacol.* 149:307–315.

Smith, I. D., and A. A. Grace. 1992. Role of the subthalamic nucleus in the regulation of the nigral dopamine neuron activity. *Synapse.* 12:287–303.

Sparks, D. L., and L. E. Mays. 1980. Movement fields of saccade-related burst neurons in the monkey superior colliculus. *Brain Res.* 190:39–50.

Steinbusch, H. W. M., and R. Niewenhuys. 1983. The raphe nuclei in the rat brainstem: a cytoarchitectonic and immunohistochemical study. *In* Chemical Neuroanatomy. P. C. Emson, editor. Raven Press, New York. 131–207.

Sugihara, G., and R. M. May. 1990. Nonlinear forecasting as a way of distinguishing chaos from measurement error in time series. *Nature (London).* 344:734–741.

Theiler, J., B. Galdrikian, A. Longtin, S. Eubank, and J. D. Farmer. 1992. Using surrogate data to detect nonlinearity in time series. *In* Nonlinear Modeling and Forecasting, Santa Fe Institute Studies in the Sciences of Complexity, Proceedings Vol. XII. M. Casdagli and S. Eubank, editors. Addison-Wesley, Reading, MA.

Tidd, C. W., L. F. Olsen, and W. M. Schaffer. 1993. The case for chaos in childhood epidemics. II. Predicting historical epidemics from mathematical models. *Proc. R. Soc. London Ser. B. Biol. Sci.* 254:257–273.

Tsonis, A. A., and J. B. Elsner. 1988. The weather attractor over very short time scales. *Nature (London).* 333:545–547.

Vives, F., and G. F. Mogenson. 1986. Electrophysiological study of the effects of D_1 and D_2 dopamine antagonists on the interaction of converging inputs from the sensory-motor cortex and substantia nigra neurons in the rat. *Neurosci.* 17:349–359.

White, G., D. M. Lovinger, and F. F. Weight. 1989. Transient low-threshold Ca^{++} current triggers burst firing through an afterdepolarizing potential in the adult mammalian neuron. *Proc. Natl. Acad. Sci. USA.* 86:6802–6806.

Wong, R. K., and M. Stewart. 1992. Different firing patterns generated in dendrites and somata of CA1 pyramidal neurones in guinea-pig hippocampus. *J. Physiol. (London).* 457:675–687.

Wong, R. K. S., and D. A. Prince. 1981. Afterpotential generation in hippocampal pyramidal cells. *J. Neurophysiol.* 45:86–97.

Yeomanns, J. S., N. T. Maidment, and B. S. Bunney. 1988. Excitability properties of the medial forebrain bundle axons of A9 and A10 dopamine neurons. *Brain Res.* 450:86–93.